Design of BSA for BCNT Device Based on 10 MeV Proton Beam Generated by Accelerator and Evaluation of Clinical Dose

Xue-wen Yan[1,2] Pei Qiao[1] De-yuan Li[1] Hua-Li[1] Li-ye Liu[1] Fa-guo Chen[1,*]

Affiliations:

[1]China Institute for Radiation Protection, Taiyuan 030006, China

[2]China Institute of Atomic Energy, Beijing 102413, China

[*]Corresponding author. *E-mail address:* chenfaguo@126.com

Abstract: The rapid development of accelerators has accelerated the clinical application of BNCT. The beam moderation and shaping assembly (BSA) in accelerator-based boron neutron capture therapy (AB-BNCT) device is crucial for the production of epithermal neutrons. Based on the 10 MeV proton beam generated by accelerator, the BSA was designed using the Monte Carlo simulation method, and the BSA design scheme was verified by the dose distribution of the epithermal neutron beam in the human head model. The results show that when the accelerator current intensity reaches 2.2 mA, the designed BSA meets the requirements of the IAEA for BNCT treatment beams. In the clinical dose estimation, the advantage depth can reach 11.2 cm, and the advantage ratio is 5. In addition, the tumor boron physical dose can reach 16 Gy within the treatment time when the normal tissue reaches the tolerance dose. The above results show that the BSA design scheme given for the 10 MeV proton beam is very reliable, and the BNCT device according to this scheme has good clinical treatment effect.

Key words: BNCT; accelerator; design of BSA; clinical dose estimation

1 Introduction

At present, cancer is the most serious public health problem in China. The latest data released by the World Health Organization in 2022 shows that the number of new cancer cases in China has reached 4.57 million, accounting for 24% of the global new cases, and the number of cancer deaths has reached 3 million, accounting for about 30% of the global deaths[1,2]. It can be seen that the demand for cancer treatment methods in China is also increasing day by day.

As an important means of cancer treatment, radiotherapy has gradually developed from traditional IMRT and VMAT, etc. to proton therapy and heavy ion therapy[3]. Although proton and heavy ion therapy has obvious advantages over traditional radiotherapy in terms of cell biological effects and treatment side effects, it has very high requirements for the positioning accuracy of tumor cells and has a relatively small clinical application range. Facing the dilemma of lacking effective treatment means for diffuse infiltrating tumors and multiple malignant tumors, BNCT has attracted more and more attention because of its advantages such as precise tumor targeting, strong biological self-adaptability, little damage to normal tissues and fewer treatment times[4].

Early BNCT used the neutron source generated by the reactor to carry out its work. With the development of accelerator technology, AB-BNCT is developing rapidly due to its small volume, being available on demand, convenient maintenance, being easy to be built in hospitals, and the fact that the neutron energy generated by accelerator is relatively low, the BSA can be set relatively small. And currently the mainstream BNCT facilities are also built based on accelerators[5-7].

AB-BNCT mainly uses a high energy accelerator to accelerate particles and then bombard the target material to generate a wide energy spectrum neutron. Then, the high energy neutron is moderated to the epithermal energy region through the BSA. Epithermal neutron is led out through the collimator to irradiate tumor cells and kill them. In the whole process, BSA is crucial for the generation of epithermal neutrons.

In this paper, the BNCT treatment device based on 10MeV proton beam generated by accelerator is designed. Through the selection of the target and the design of BSA, the epithermal neutron beam is obtained, and the parameters of the epithermal neutron beam at the BSA beam exit port are simulated and calculated. In addition, the dose parameters of BSA beam exit are evaluated by constructing the human head model, which provides theoretical calculation support for clinical treatment.

2 Materials and methods

2.1 Design requirements of BSA

IAEA released "ADVANCES IN BORON NEUTRON CAPTURE THERAPY"[8] in June 2023, which gives specific recommended values for the performance of BNCT epithermal neutrons. In this paper, the detailed design of BSA is carried out according to IAEA recommended values. The specific indicators are shown in Table 1.

Table 1. Design Indicators of BNCT Neutron Beam Parameters (IAEA)

Beam Parameter	Design Indicator
φ_{epi}	$\geq 5.0\times10^{8}$ cm$^{-2}\cdot$s^{-1}
$\varphi_{th}/\varphi_{epi}$	≤ 0.05
D_{γ}/φ_{epi}	$\leq 2\times10^{-13}$ Gy$\cdot$cm^{2}
D_{fast}/φ_{epi}	$\leq 7\times10^{-13}$ Gy$\cdot$cm^{2}
$\varphi_{epi}/\varphi_{total}$	$\geq 85\%$

2.2 Selection of target

At present, the mainstream methods for generating epithermal neutrons in BNCT are based on the $^{7}Li(p, n)^{7}Be$ and $^{9}Be(p, n)^{9}B$ reactions, and these two methods have a strong dependence on the accelerator energy[9] . The advantage of the Li target is that it has a higher neutron yield than the Be target at a relatively low proton beam energy (for example, 2.5 MeV - 3.5 MeV), and the neutron energy is also low and easy to moderate. However, the disadvantage of the Li target is its low melting point (< 180 °C). In order to maintain its performance and extend its service life, how to conduct away the power deposited by the high power proton hitting the target is a rather difficult technical problem. The Be target has a high melting point, which can reach 1287 °C, and has relatively good thermal conductivity. However, the Be target has a low neutron yield. In order to achieve the required neutron flux, the proton energy hitting the target generally needs to be greater than 5MeV[10] .

The accelerator used in this paper can accelerate protons to 10 MeV. Therefore, the Be target is selected as the designed target material. According to the size of the beam pipeline, the radius of the Be target is designed to be 2.5 cm, and then the thickness of the target is designed using the Monte Carlo program. Fig. 1 shows the neutron yield at different thicknesses.

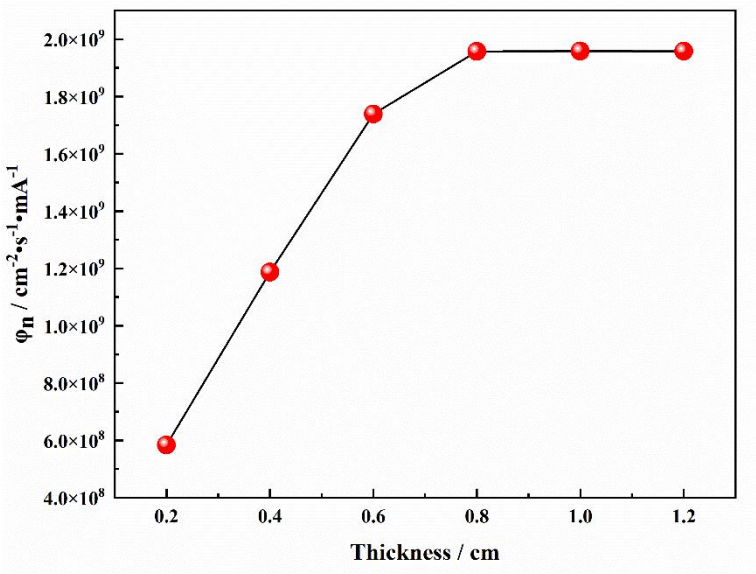

Fig.1. Neutron yield of Be targets with different thicknesses bombarded by 10 MeV protons

The results in Fig. 1 show that when the thickness of the Be target reaches 800 μm, the neutron yield tends to be flat. Therefor, the thickness of the Be target is designed to be 800 μm considering that as the thickness of the Be target increases, more heat will be deposited in the target. The

outgoing neutron energy spectrum is shown in Fig. 2.

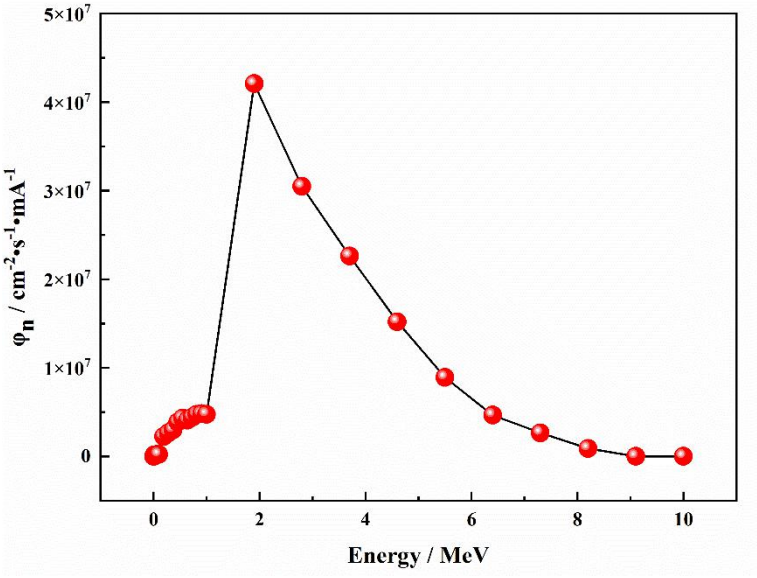

Fig.2. Outgoing neutron energy spectrum of 800 μm Be target bombarded by 10 MeV protons

It can be seen from Fig. 2 that the proportion of epithermal neutrons generated by 10 MeV protons bombarding the Be target is extremely small, and most of the neutron energies are above 1 MeV. They must be moderated before used for BNCT treatment.

2.3 Design of BSA

BSA mainly consists of reflector layer, fast neutron filter layer, main moderator layer, thermal neutron absorber layer, γ absorber layer and collimator[7]. The specific structure of BSA is shown in Fig. 3.

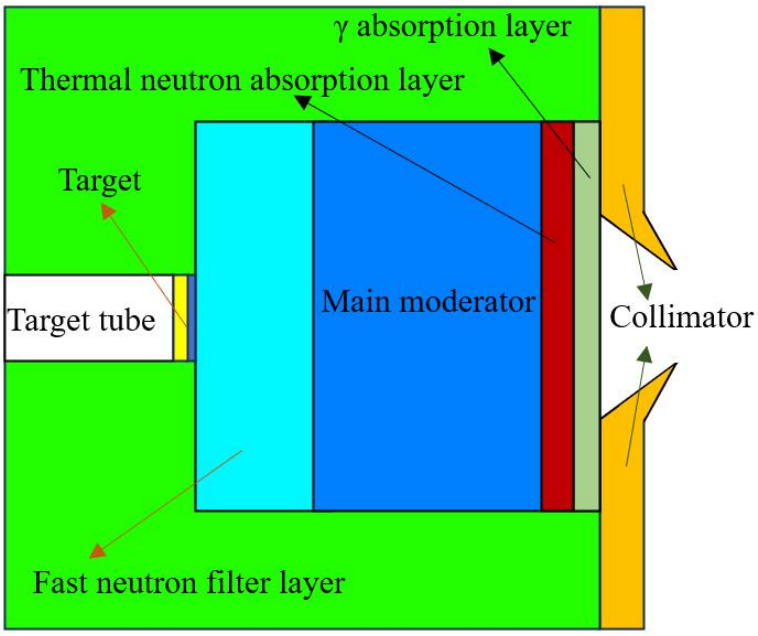

Fig.3. Schematic diagram of BSA structure

2.3.1 Design of the fast neutron filter layer

The fast neutron filter layer mainly filters out the high energy neutrons generated by target, so that more fast neutrons are filtered out before entering the subsequent main moderator. In order to filter out the neutrons with energy of several MeV, Fe with medium atomic number is selected as the filter material. Because of its high density and high neutron absorption cross section, Fe can rapidly reduce the fast neutron energy below 1 MeV through inelastic scattering.

Simulating and calculating the neutron beam situation of 10 MeV protons bombarding the Be target and then passing through Fe filters with different thicknesses by Monte Carlo program. The initial input parameters are as follows: the thickness of the Be target is 0.8 mm, the diameter is 2.5 cm, the overall structure of BSA is cylindrical along the beam line direction, and the radius of the fast neutron filter layer is 40 cm. Fig. 4 shows the neutron energy spectra after the emitted neutrons pass through Fe filters with different thicknesses. Fig. 5 shows the proportion and flux data of neutrons below 1 MeV.

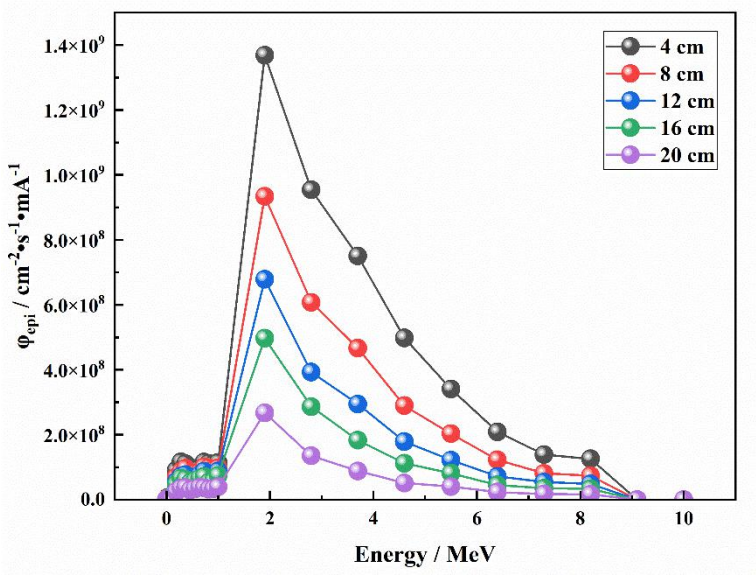

Fig.4. Neutron energy spectra of emitted neutrons after being filtered by Fe with different thicknesses

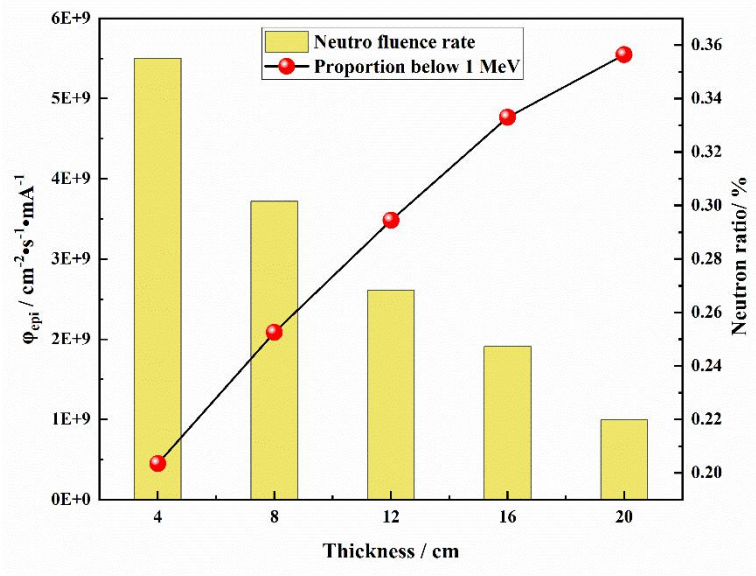

Fig.5. Proportion of neutrons below 1 MeV and neutron flux

It can be seen from Fig. 4 and Fig. 5, after passing through Fe filters with different thicknesses, the neutron energy spectra do not change significantly. However, as the thickness of the Fe filter increases, the proportion of neutrons below 1 MeV increases significantly. These results show that Fe filter can quickly reduce the fast neutron energy to below 1 MeV. Nevertheless, as the thickness of the Fe filter increases, the neutron flux also decreases significantly, which has a great impact on the final epithermal neutron flux. Therefore, the thickness of the Fe filter should not be set too thick, and the proportion of neutrons below 1 MeV and the neutron flux should be considered comprehensively.

2.3.2 Design of the main moderator

The main moderator is the core component of BSA. Its function is to further slowdown the neutrons with lower energy after passing through the filter to epithermal neutron and thermal neutron energy regions.

① Material selection

Through a large number of investigations, it is found that research institutions such as the University of Tsukuba and Kyoto University in Japan, IBA in Belgium, TAE in the United States, BINP in Russia, INFN in Italy, and the Shanghai Institute of Applied Physics of the Chinese Academy of Sciences have used moderating materials such as D_2O, graphite, MgF_2, TiF_3, LiF, AlF_3, and Fluental in the design of AB-BNCT through investigation[11-15]. Considering comprehensively in terms of performance, price, and material availability, this paper selects MgF_2, TiF_3, and AlF_3 as

alternative materials for the main moderator of BSA. Then, the properties of the three candidate materials are calculated and analyzed from three aspects: epithermal neutron fluence rate, fast neutron fluence rate and thermal neutron fluence rate. φ_{epi}, $\varphi_{epi}/\varphi_{fast}$, and $\varphi_{th}/\varphi_{epi}$ are shown in Fig. 6.

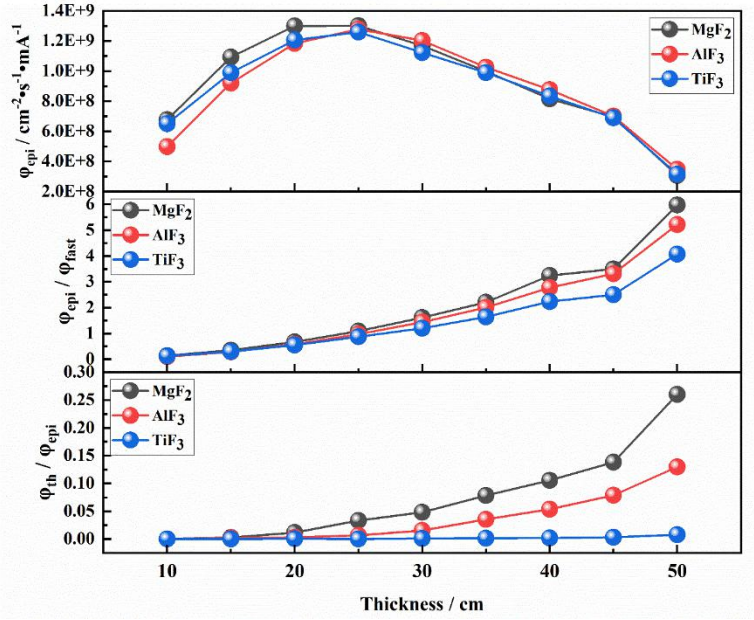

Fig.6. φ_{epi}, φ_{epi} / φ_{fast}, φ_{th} / φ_{epi} of three moderating materials at different thicknesses

Fig. 6 shows that when the thickness of the moderators is the same, the epithermal neutron flux of MgF_2 is basically the highest, and it has the best neutron moderating effect (both $\varphi_{epi}/\varphi_{fast}$ and $\varphi_{th}/\varphi_{epi}$ are the largest). Therefore, MgF_2 has the best moderating performance among the three materials. However, if the designed thickness of the MgF_2 material is too large, it will lead to too high proportion of thermal neutrons, and the over moderation situation needs to be considered in the design.

② The thickness design of the main moderator

The recommended value of BNCT treatment beams in IAEA is $\varphi_{th}/\varphi_{epi} \leq 0.05$. Combined with Fig. 6, when the thickness of MgF_2 is 30 cm, the value of $\varphi_{th}/\varphi_{epi}$ is approximately equal to 0.05. Considering the fast neutron filter layer will be added later, it is more appropriate to take the initial thickness of MgF_2 as 35 cm to 40 cm, and then fine tune according to the beam parameters after adding each functional layer. In addition, the radius of the main moderator is 40 cm.

③ Thickness design of the fast neutron filter layer

Fe filter was added in front of the main moderator MgF_2 with thickness of 40 cm, and the shooting situation was recorded by changing the thickness of the Fe filter. The results show that

when the thickness of the Fe filter is 14 cm, $\varphi_{epi}/\varphi_{fast}$ can reach about 20, and $\varphi_{th}/\varphi_{epi}$ can reach about 0.04. Therefore, the thickness of the Fe filter is initially selected as 15 cm in this design, and subsequent fine tuning will be carried out according to the calculation results.

2.3.3 Design of thermal neutron absorption layer

The function of the thermal neutron absorption layer is to absorb the low energy thermal neutrons that pass through the main moderator. Cd is a commonly used thermal neutron absorbing material[16]. It has a large thermal neutron absorption cross section, but using it as a thermal neutron absorbing material will generate secondary γ radiation, which will contaminate the epithermal neutron field. Therefore, the shielding of secondary γ rays should be considered.

The fluence ratios of thermal neutrons to epithermal neutrons for different thicknesses of Cd layers are obtained through Monte Carlo calculations. In the calculations, the thickness of MgF_2 is taken as 40 cm, and the thickness of Fe is taken as 14 cm. The detailed results of the above contents are shown in Fig. 7.

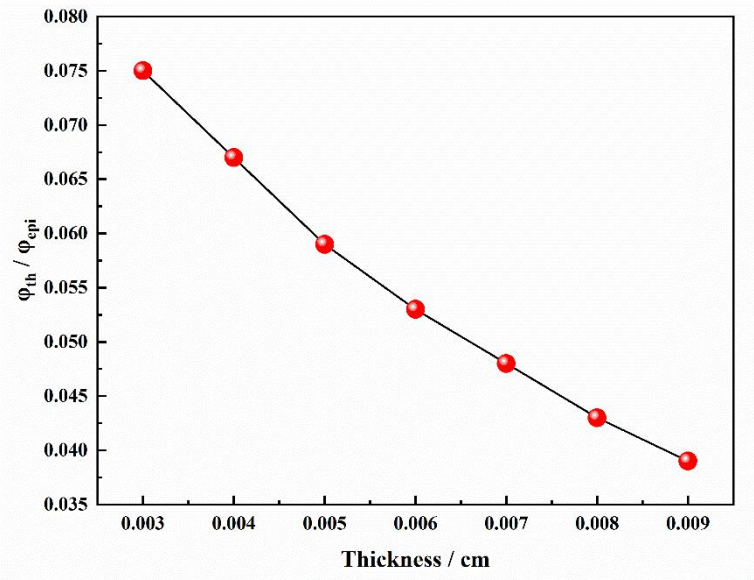

Fig.7. $\varphi_{th}/\varphi_{epi}$ under different thicknesses of Cd layers.

According to the results in Fig. 7, when the thickness of Cd is above 0.007 cm, the values of $\varphi_{th}/\varphi_{epi}$ all meet the recommended values of the IAEA ($\varphi_{th}/\varphi_{epi} \leq 0.05$).

2.3.4 Design of γ absorbing layer

The secondary γ radiation will be generated in the processes of inelastic scattering of fast neutrons and absorption of thermal neutrons, which will contaminate the epithermal neutron field. The function of the γ absorption layer is to purify the epithermal neutron radiation field and remove

the secondary γ rays in the radiation field. Usually, Pb and Bi are used to absorb the γ rays. Pb is superior to Bi in terms of γ absorption, but Bi has an advantage over Pb in terms of neutron penetration[17]. Therefore, Bi is the optimal choice when a higher neutron fluence is required.

In the Monte Carlo calculations, the thickness of MgF_2 is taken as 40 cm, the thickness of Fe is taken as 14 cm, and the thickness of Cd is taken as 0.007 cm. The ratio of the γ dose to the epithermal neutron fluence for different thicknesses of Bi layers is shown in Fig. 8.

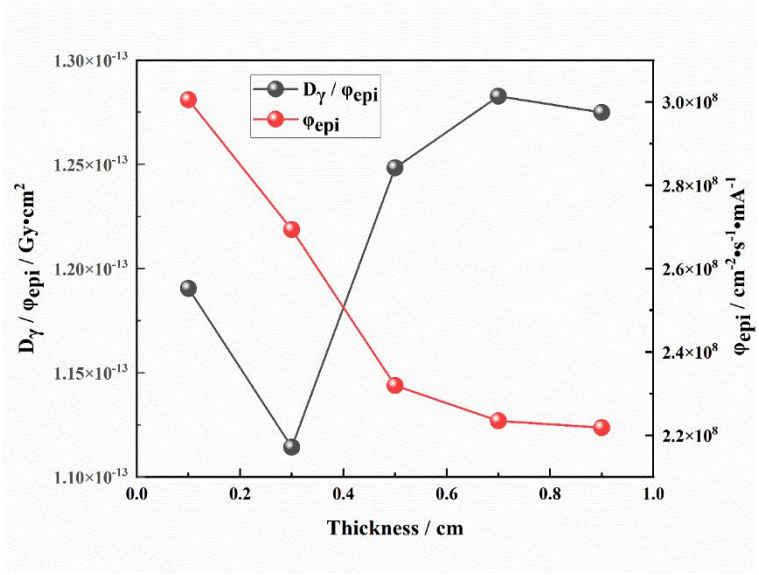

Fig.8. D_γ/φ_{epi} and φ_{epi} under different thicknesses of Bi layers.

According to the data in Fig. 8, as the thickness of the Bi layer increases, the epithermal neutron fluence decreases correspondingly, and the ratio of the γ dose to the epithermal neutron fluence shows an upward trend, which indicating that Bi will not only absorb γ but also reduce the epithermal neutron fluence. Therefore, the thickness of the Bi layer should not be designed too thick. After comprehensive consideration, when it is set to 0.3 cm, the value of D_γ/φ_{epi} meets the recommended value of the IAEA ($D_\gamma/\varphi_{epi} \leq 2\times10^{-13}$ Gy·cm²), and φ_{epi} is relatively high.

2.3.5 Design of the reflector layer

The function of the reflector layer is to reflect and converge the neutrons generated by the target system towards the exit direction and to shield the secondary γ rays. It is necessary to take into account both the reflection of backward neutrons and the shielding of secondary γ rays generated at the same time. Lead material is usually used as the reflector material.

In the Monte Carlo calculation, the radius of the Pb in the reflector layer is selected to be 50 cm, and the thickness of the Pb layer in the opposite direction of the proton beam is calculated from 15

cm to 40 cm with a step length of 5 cm. Under this condition, the epithermal neutron fluence parameters at the BSA beam exit are obtained, and the specific situation is shown in Fig. 9.

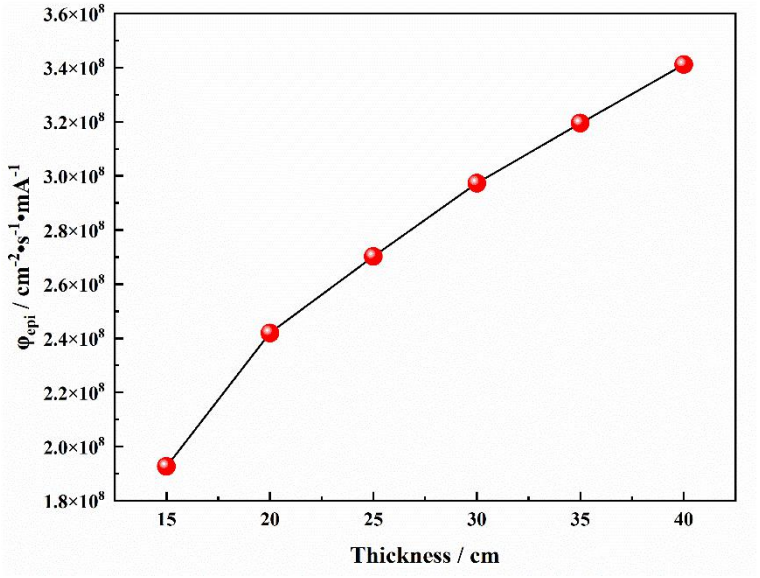

Fig.9. Epithermal neutron fluence of Pb reflector layers with different thicknesses in the opposite direction of the proton beam

It can be seen from Fig. 9 that as the thickness of the reflector layer increases, the epithermal neutron fluence gradually increases. But the magnitude of the increase gradually decreases. Therefore, considering the cost and the degree of performance improvement comprehensively, Pb with a thickness greater than 20 cm is selected as the design thickness of the reflector layer in the reverse direction of the proton incident direction.

The reflector layer in the opposite direction of the axial beam is designed to be 20 cm, and the epithermal neutron fluxes at different radii of the radial reflector of the main moderator are obtained through modeling. The detailed results are shown in Fig. 10.

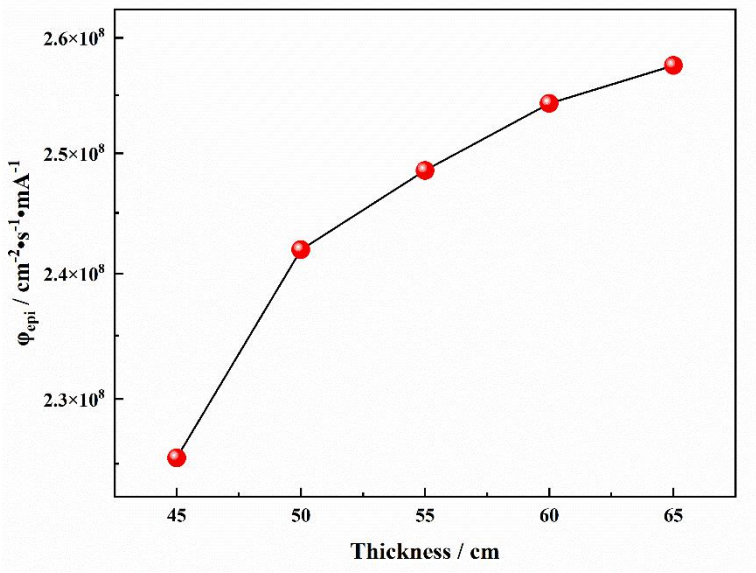

Fig.10. Epithermal neutron fluence of Pb reflector layers with different radii

It can be seen from Fig. 10 that as the radius of the main moderator reflector layer increases, the epithermal neutron fluence shows an increasing trend, and the rate of increase slows down when the radius is greater than 50 cm. Therefore, it is more appropriate to design the thickness of the main moderator radial reflector layer as 50 cm.

2.3.6 Design of the collimator

The center of the collimator along the beam path is usually an air filled cavity. The downstream part of the collimator focuses the neutrons in the cavity to the beam exit. Therefore, a conical channel used Pb is set at the beam exit position[18], and the polyethylene containing boron is set outside the beam exit to achieve epithermal neutron collimation.

3 Results and Discussions

3.1 Performance Evaluation of BSA

BSA design scheme that meets the recommended values of the IAEA is obtained by fine tuning the thickness of each functional layer. The overall performance parameters of BSA are evaluated based on the Monte Carlo program. The specific design parameters are shown in Table 2, and the performance parameters of the neutron field at BSA beam exit are shown in Table 3.

Table 2. Design parameters of BSA

Number	Functional Layer	Material	Density / g/cm^{-3}	Thickness /cm	Radius /cm	Remarks
1	fast neutron filter layer	Fe	7.15	15	40	

2	main moderator	MgF_2	3.10	39	40	
3	thermal neutron absorption layer	Cd	8.65	0.07	40	
4	γ absorbing layer	Bi	9.8	0.3	40	
5	reflector layer	Pb	11.34	20	50	
6	collimator	Pb	11.34	7	50	cone angle-30°; outer diameter-14 cm
		polyethylene (B_4C-10%)	1.00	2	/	Radial width-5 cm

Table 3. Neutron field parameters at the beam exit of BSA

Parameter Type	φ_{epi}	$\varphi_{th}/\varphi_{epi}$	$\varphi_{epi}/\varphi_{total}$	D_γ/φ_{epi} /Gy·cm²	D_{fast}/φ_{epi} /Gy·cm²
IAEA recommended value	5×10^8 cm^{-2}·s^{-1}	≤ 0.05	≥ 85%	≤ 2×10^{-13}	≤ 7×10^{-13}
Design value	2.32×10^8 cm^{-2}·s^{-1}·mA^{-1}	0.042	92.5%	1.25×10^{-13}	6.75×10^{-13}

It can be seen from the data in Table 3 that when the current intensity of the accelerator reaches above 2.2 mA, all parameters of the neutron field at the beam exit can reach the IAEA recommended values after being moderated by the BSA.

According to the design parameters in Table 2, the energy spectrum and spatial distribution of epithermal neutrons at the beam exit are given through modeling and calculation, and the specific results are shown in Fig. 11.

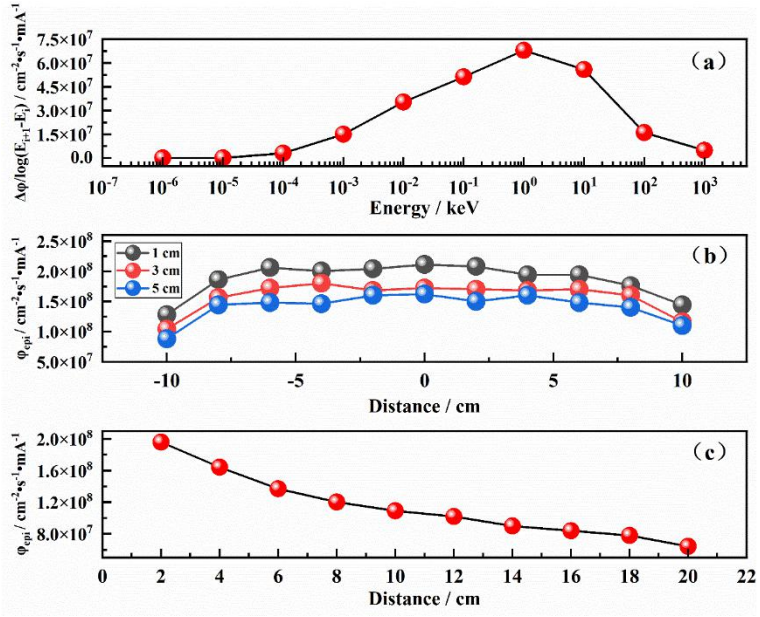

Fig.11. Neutron beam parameters at BSA Beam Exit ((a) Neutron energy spectrum; (b) Radial distribution of epithermal neutrons; (c) Axial distribution of epithermal neutrons)

Fig. 11 shows that the neutron energy emitted through BSA is mainly concentrated in the range of epithermal (0.5 eV - 10 keV). And the fluence rate is relatively high within the diameter range of 14 cm at the beam exit. When the radius exceeds -7 cm and +7 cm, the epithermal neutron fluence decreases significantly. As the distance from the beam exit position increases, the epithermal neutron fluence generally shows a downward trend. Within the diameter range of 14 cm, the radial distribution of the epithermal neutron fluence is relatively consistent, and the radial average relative error is about 8.5% at the position 1 cm away from the beam exit. In addition, at the position of 3 cm, the average relative error is approximately 6.7%, and at the position of 5 cm, the average relative error is approximately 8.6%. Fig. 11(c) shows that along the beam direction, as the distance from the beam exit increases, the epithermal neutron fluence gradually decreases. The above results are consistent with the theory, which shows that the BSA in this paper meets the design objectives.

3.2 Evaluation of clinical dose

Dose estimation in BNCT is completely different from that in photon and electron therapies. Its dose composition includes four parts: Boron dose (D_B), Proton dose (D_p), Neutron dose (D_n) and γ dose (D_γ). The above four doses have different relative biological effects[19].

D_B comes from α and Li particles produced by the $^{10}B(n,\alpha)^7Li$ reaction. Their average ranges are 8.9 μm and 4.8 μm respectively, and they can deposit all their energy within the cell. D_p mainly comes from the proton dose produced by the $^{14}N(n,p)^{14}C$ reaction. D_n is mainly the neutron dose of fast neutrons and epithermal neutrons. D_γ comes from the γ dose produced by the $^1H(n,\gamma)^2D$ reaction [20].

The weighted total dose of biological effects in BNCT is the sum of products of four absorbed doses and corresponding biological effect weighting factors[21,22].

$$D_{RBE} = CBE_B \times D_B + RBE_n \times D_p + RBE_n \times D_n + RBE_\gamma \times D_\gamma \quad (1)$$

In formula(1), RBE is the relative biological effect factor, and CBE is the compound biological effectiveness factor. The values of each parameter: RBE_p= 1.0, RBE_n= 3.2, CBE_B= 3.8 for tumor tissues, and CBE_B= 1.35 for normal tissues[23-25].

In order to study the dosimetric parameters at the beam exit of the BNCT treatment device designed in this paper, Snyder modified head model is used to calculate the dose.

3.2.1 Modeling of Snyder modified head model

In the Snyder modified human head model[26-29], the interfaces between the scalp, skull, and brain are defined by the following three equations:

$$(x \quad /6)^2 + (y \quad /9)^2 + ((z \quad -1)/6.5)^2 = 1 \tag{2}$$

$$(x \quad /6.8)^2 + (y \quad /9.8)^2 + (z \quad /8.3)^2 = 1 \tag{3}$$

$$(x \quad /7.3)^2 + (y \quad /10.3)^2 + (z \quad /8.8)^2 = 1 \tag{4}$$

Modeling the Snyder modified human head model according to formula(2), formula(3) and formula(4). The tissue densities used in the modeling are taken from ICRU- 46 Report[30]. The detailed model is shown in Fig. 12.

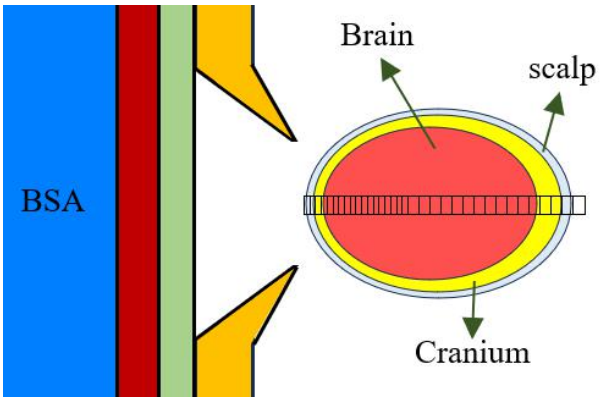

Fig.12. Diagram of Snyder modified human head model

Dose calculation is mainly carried out along the central axis of the head model. A cylindrical detector with a radius of 0.8 cm is established to record the doses of each component at different depths in the head model. Among them, the step size is 0.1cm in the range of 0 cm to 2 cm, the step size is 0.2 cm in the range of 2 cm to 4 cm, the step size is 0.4cm in the range of 4 cm to 8 cm, and the step size is 0.8 cm in the range of 8 cm to 16 cm. In calculation, the boron concentration in normal tissues is 18 ppm, and that in tumor tissues is 65 ppm[31].

3.2.2 Results of dose estimation

Using Kerma factor[32- 34] to convert the flux into dose, and plotting the graph to shown dose results at all positions in Fig. 13.

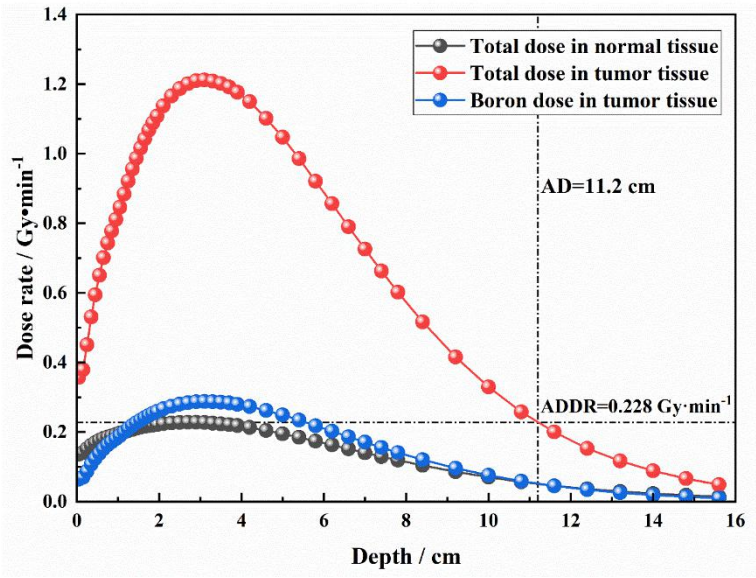

Fig.13. Dose distribution in the Snyder modified human head model

The results in Fig. 13 shows that the advantage depth (AD) of the neutron beam in the beam exit of the BNCT treatment device designed in this paper is 11.2 cm. The maximum dose rate in normal tissues (ADDR) is 0.228 Gy·min^{-1}. The longest allowable treatment time (TT) [35] is 54.82 min, and the advantage ratio (AR) is 5.

Combined with the treatment time (TT) and the boron dose curve of tumor tissues in Fig. 13, the results show that within the longest allowable treatment time, the peak value of the tumor boron dose can reach 16 Gy. Which is higher than the requirement of a tumor boron dose greater than 15 Gy in BNCT clinical treatment[36], and theoretically has a relatively good treatment effect.

4 Summary

In response to the urgent need for AB-BNCT treatment devices, this paper selected the ^{9}Be(p, n)^{9}B design scheme and designed the corresponding BSA based on the 10 MeV proton beam generated by accelerator. After calculation, the neutron beam parameters at the exit meet the IAEA's index requirements for BNCT beam parameters. Meanwhile, a Synder modified human head model was constructed to evaluate the BNCT dose. The results show that the BNCT treatment device designed in this paper has a relatively good advantage depth. At the advantage depth of 11.2 cm, almost all head tumors can be treated, and within the treatment time when the normal tissues reach the tolerance dose, the physical boron dose in the tumor can reach 16 Gy, which has a very good treatment effect. The research results of this paper can provide a theoretical design basis for BNCT treatment devices based on accelerator.

References:

[1] Freddie Bray BSc, Mathieu Laversanne, Hyuna Sung, et al. International Journal of Cancer. Global Cancer Statistics 2022: GLOBOCAN estimates of incidence and mortality worldwide for 36 cancers in 185 countries[J]. A Cancer J Clin. 2024;74:229–263. https://doi.org/10.3322/caac.21834.

[2] Zheng Rongshou, Chen Ru, Han Bingfeng, et al. Cancer incidence and mortality in China, 2022[J]. Chinese Journal of oncology. 2024, 46(03): 221-231. https://doi.org/10.3760/cma.j.cn112152-20240119-00035.

[3] XY Su, PD Liu, W Hao, et al. Enhancement of radio sensitization by metal-based nanoparticles in cancer radiation therapy[J]. Cancer Biology & Medicine, 2014, 2(11): 86-91. https://doi.org/10.7497/j.issn.2095-3941.2014.02.003.

[4] Coderre J A, Morris G M. The radiation biology of boron neutron capture therapy[J]. Radiat Res, 1999, 151: 1–18. https://doi.org/10.2307/3579742.

[5] Yi-Nan Zhu, Zuo-Kang Lin, Hai-Yan Yu, et al. Study on the optimal incident proton energy of 7Li(p, n)7Be neutron source for boron neutron capture therapy[J]. Nuclear Science and Techniques, 2024, 35(60). https://doi.org/10.1007/s41365-024-01420-6.

[6] Yoshioka M. Review of accelerator-based boron neutron capture therapy machines. Proc Int Part Accelerat Conf, 2016, THXB01: 3171–3175. https://doi.org/10.18429/JACOW-IPAC2016-THXB01.

[7] Kreiner A J, Bergueiro J, Cartelli D, et al. Present status of accelerator-based BNCT. Rep Pract Oncol Radiother, 2016, 21: 95−101. https://doi.org/10.1016/j.rpor.2014.11.004.

[8] LW Wang. Editorial: Recent advances in boron neutron capture therapy in radiation oncology[J]. Frontiers in Oncology. 2024, https://doi.org/10.3389/fonc.2024.1398781.

[9] Ali Pazirandeh, Sahar Naserbakht. Design and Simulation of a Neutron Generating Target Based on the 9Be (P, N) 9B Reaction for Use in BNCT[J]. Journal of Scientific & Technical Research, 2022. DOI: 10.26717/BJSTR.2022.42.006795. https://doi.org/10.26717/bjstr.2022.42.006795.

[10] Fu S N, Liang T J, Chen H S. Status and outlook: Research and development on the neutron source for BNCT. Chin Sci Bull, 2022, 67: 1471– 1478. https://doi.org/10.1360/TB-2021-1254.

[11] Rasouli F S, Masoudi S F, Kasesaz Y. Design of a model for BSA to meet free beam parameters for BNCT based on multiplier system for D-T neutron source[J]. Annals of Nuclear Energy, 2012, 39(1): 18 –25. https://doi.org/10.1016/j. anucene.2011.08.025.

[12] C. Ceballos, J. Esposito, S. Agosteo, et al. Towards the final BSA modeling for the accelerator-driven BNCT facility at INFN LNL[J]. Applied Radiation and Isotopes, 69 (2011) 1660-1663. https://doi.org/10.1016/j.apradiso.2011.01.032.

[13] H. Tanaka, Y. Sakurai, M. Suzuki, et al. Characteristics comparison between a cyclotron-based neutron source and KUR-HWNIF for boron neutron capture therapy[J]. Nuclear Instruments and Methods in Physics Research B, 267 (2009) 1970–1977. https://doi.org/10.1016/j.nimb.2009.03.095.

[14] Hiroaki KUMADA, Fujio NAITO, Kazuo HASEGAWA, et al. Development of LINAC-Based Neutron Source for Boron Neutron Capture Therapy in University of Tsukuba[J]. Plasma and Fusion Research: Regular Articles, 13, 2406006 (2018). https://doi.org/10.1585/pfr.13.2406006.

[15] Yi-Nan Zhu, Zuo-Kang Lin, Hai-Yan Yu, et al. Study on the optimal incident proton en ergy of Li(p, n)7Be neutron source for boron neutron capture therapy[J]. Nuclear Scienc e and Techniques, 2024, 35: 60, h https://doi.org/10.1007/s41365-024-01420-6.

[16] Hiroaki KUMADA, Fujio NAITO, Kazuo HASEGAWA, et al. Development of LINAC-Based Neutron Source for Boron Neutron Capture Therapy in University of Tsukuba[J]. Plasma and Fusion Research: Regular Articles, Volume 13, 2406006 (2018). https://doi.org/10.1585/pfr.13.2406006.

[17] GUO Zhiqi, LIU Changqi, ZHANG Weizhong, et al. Optimization design of BNCT neutron source and moderating body based on accelerator 7Li(p, n) reaction[J]. NUCLEAR TECHNIQUES, 2022, 45(5): 050201. https://doi.org/10.11889/j.0253-3219.2022.hjs.45.050201.

[18] Naonori Hu, Hiroki Tanaka, Ryo Kakino, et al. Improvement in the neutron beam collimation for application in boron neutron capture therapy of the head and neck region[J]. scientific reports. 2022, 12: 13778. https://doi.org/10.1038/s41598-022-17974-7.

[19] . Wolfgang A.G. Sauerwein, Andrea Witting, Raymon Moss, et al. Neutron Capture Therapy: Principles and Applications[M]. Springer-Verlag Berlin Heidelberg, 2012.

https://doi.org/10.1049/ep.1966.0160.

[20] . GOORLEY J T, KIGER W S, ZAMENHOF R G, et al. Reference dosimetry calculations for neutron capture therapy with comparison of analytical and voxels models[J]. Medical Physics, 2002,29(2): 145-156. https://doi.org/10.1118/1.1428758.

[21] . WANG Yongquan, Wang Zezhen, LI Ning, et al. Design of Beam Shaping Assembly for Accelerator-based Boron Neutron Capture Therapy and Study on Its Clinical Parameter[J]. Atomic Energy Science and Technology, 2022,56(7): 1440-1447 (in Chinese). https://doi.org/10.7538/yzk.2021.youxian.0467.

[22] Zhaopeng Qiao, Baolong Ma, Bo Rong, et al. Beam shaping assembly design of Li(p,n) neutron source with a rotating target for boron neutron capture therapy[J]. Nuclear Instruments and Methods in Physics Research Section A: Accelerators, Spectrometers, Detectors and Associated Equipment, Volume 1052,2023,168249,ISSN 0168-9002, https://doi.org/10.1016/j.nima.2023.168249.

[23] CODERRE J, MAKAR M, MICCA P, et al. Derivations of RBE for the high-LET radiations produced during boron neutron capture irradiation of the 9L rat gliosarcoma in vitro and in vivo[J]. International Journal of Radiaton Oncology Biology Physics, 1993, 27(5): 121-129. https://doi.org/10.1016/0360-3016(93)90023-9.

[24] Qiao ZP, Hu YC, Jiang QX, et al. Coin-structured Tunable Beam Shaping Assembly Design for Accelerator-Based Boron Neutron Capture Therapy for Tumors at Different Depths and Scales [J]. Nuclear Science and Techniques, 2023, 34: 186. https://doi.org/10.1007/s41365-023-01325-w.

[25] LEE C L, ZHOU X, KUDCHADKER R J, et al. A Monte Calor dosimetry-based evaluation of the 7Li(p, n)7Be reaction near threshold for accelerator boron neutron capture[J]. Medical Physics, 2000, 27(1): 192-202. https://doi.org/10.1118/1.598884.

[26] Snyder W S, Fisher H L J, Ford M R, et al. Estimates of absorbed fractions for monoenergetic photon sources uniformly distributed in various organs of a heterogeneous phantom [J]. Journal of Nuclear Medicine,1969,10(3):Suppl 3:7-52. https://doi.org/10.1016/0014-5793(74)80747-7.

[27] Hawthorne M F, Shelly K, Wiersema R J. Frontiers in Neutron Capture Therapy[M]. Kluwer Academic/Plenum Publishers, 2001. ISBN：978-1-4613-5478-9.

[28] Goorley J T, Kiger W S, Zamenhof R G. Reference dosimetry calculations for Neutron Capture Therapy with comparison of analytical and voxel models[J]. Medical Physics,2002,29(2):145-156. https://doi.org/10.1118/1.1428758.

[29] F. Rahmani, M. Shahriari, Dose calculation and in-phantom measurement in BNCT using response matrix method. Appl. Radiat. Isot. 69, 1874–1877 (2011). https://doi.org/10.1016/j.apradiso.2011.02.019.

[30] ICRU 46, Photon, electron, proton, and neutron interaction data for body tissue[R]. Bethesda: International Commission on Radiation Units and Measurements, 1992.

[31] Kononov O E, Kononov V N, Bokhovko M V, et al. Optimization of an accelerator-based epithermal neutron source for neutron capture therapy[J]. Applied Radiation and Isotopes, 2004, 61(5): 1009-1013. https://doi.org/10.1016/j.apradiso.2004.05.028.

[32] ICRU 63. Nuclear data for neutron and proton radiotherapy and for radiation protection[R]. Bethesda: International Commission on Radiation Units and Measurements, 2000.

[33] SELTZER S, Calcuation of photon mass energy transfer and mass energy-absorption coefficients[J]. Radiation Research, 1993,136(2): 147-170. https://doi.org/10.2307/3578607.

[34] WANG Yongquan, WANG Zezhen, LI Ning, et al. Design of Beam Shaping Assembly for Accelerator-based Boron Neutron Capture Therapy and study on Its Clinical Parameter[J]. Atomic Energy Science and Technology, 2022,56(7): 1440-1447 (in Chinese). https://doi.org/10.7538/yzk.2021.youxian.0467.

[35] N. Hu, H. Tanaka, K. Ono, Design of a filtration system to improve the dose distribution of an accelerator-based neutron capture therapy system. Med. Phys. 49(10), 6609–6621 (2022). https://doi.org/10.1002/mp.15864.

[36] WOLFGANG A G S, ANDREA W R M, YOSHINOBU N. Neutron capture therapy principles and application[M]. Heidelberg: Springer, 2012: 363-364. https://doi.org/10.1007/978-3-642-31334-9.